

Zhang, K., Wang, H., Yamazaki, Y. (2022): Effects of Subauroral Polarization Streams on the Equatorial Electrojet During the Geomagnetic Storm on 1 June 2013: 2. The Temporal Variations. - Journal of Geophysical Research: Space Physics, 127, e2021JA030180.

<https://doi.org/10.1029/2021JA030180>

JGR Space Physics

RESEARCH ARTICLE

10.1029/2021JA030180

This article is a companion to Zhang et al. (2021), <https://doi.org/10.1029/2021JA029681>.

Key Points:

- ubauroral polarization streams-induced counter equatorial electrojet (CEJ) shows a 2–3 hr delay with respect to SAPS
- The time delay of CEJ attributes to the traveling atmospheric disturbances in zonal winds
- The effects of meridional winds on CEJ depend greatly on the geomagnetic declination

Correspondence to:




H. Wang,
h.wang@whu.edu.cn

Citation:

Zhang, K., Wang, H., & Yamazaki, Y. (2022). Effects of subauroral polarization streams on the equatorial electrojet during the geomagnetic storm on 1 June 2013: 2. Temporal variations. *Journal of Geophysical Research: Space Physics*, 127, e2021JA030180. <https://doi.org/10.1029/2021JA030180>

Received 2 DEC 2021
Accepted 10 JAN 2022

Effects of Subauroral Polarization Streams on the Equatorial Electrojet During the Geomagnetic Storm on 1 June 2013: 2. The Temporal Variations

Kedeng Zhang¹ , Hui Wang¹ , and Yosuke Yamazaki² 

¹Department of Space Physics, School of Electronic Information, Wuhan University, Wuhan, China, ²Helmholtz Centre Potsdam, GFZ German Research Centre for Geosciences, Potsdam, Germany

Abstract Using ground-based magnetic field measurements and numerical simulations from the Thermosphere-Ionosphere Electrodynamics General Circulation Model (TIEGCM), a first paper (Zhang, Yamazaki, et al., 2021, doi: <https://doi.org/10.1029/2021JA029681>; under review) introduced the potential roles of disturbance dynamo electric field due to subauroral polarization streams (SAPS) on the equatorial electrojet (EEJ) during a moderate geomagnetic storm on 1 June 2013. Our second study investigated the temporal responses of equatorial electrojet to SAPS. At noon, the residual EEJ (Δ EEJ) owing to SAPS flows westward, that is, counter equatorial electrojet (CEJ). The temporal variation of CEJ excited by the dynamo electric field was basically consistent with that by SAPS, and the effects of zonal wind were larger than those of meridional wind. The relative time delay of CEJ and SAPS was related to the propagation time of disturbance wind from mid-latitudes to low-latitudes. It took 2–3 hr for SAPS-related disturbance wind to propagate to the equatorial region and change the polarity of EEJ. The influence of meridional winds on the temporal variations of Δ EEJ is related to the generation of eastward currents at mid-latitudes, which can accumulate the positive charges at dusk terminator and then generate a westward electric field at lower latitudes.

Plain Language Summary The equatorial electrojet (EEJ) represents a ribbon of intense electric current flowing in the ionospheric E region (approximately 110 km) on the dayside along the dip equator. Its behaviors are controlled by the daytime ionospheric electric field and ionospheric conductivity. However, the temporal variations of EEJ in response to the subauroral polarization streams (SAPS), an interesting and important physical phenomenon at subauroral latitudes, are seldom explored and poorly understood. The understanding of EEJ behaviors and their associated physical drivers during SAPS periods can contribute to the modeling and forecasting of the equatorial space environment, and the understanding of the coupling between ionosphere-thermosphere systems at high-latitudes and dip equator.

1. Introduction

In the equatorial ionosphere, a number of special and interesting physical phenomena, such as, post-sunset equatorial plasma bubbles/depletions (Burke et al., 2004; Wan et al., 2018), zonal wind jet (Liu et al., 2016), equatorial electrojet (EEJ, eastward), and counter-equatorial electrojet (CEJ, westward; Alken & Maus, 2010; Lühr et al., 2008; Wang et al., 2019; Yamazaki et al., 2017), have been reported. Since the discovery of EEJ and CEJ, which are intense currents at an altitude of 105–110 km and are confined to a narrow band along the dip equator, the study of their behaviors has been a key topic in understanding the modeling and forecasting of the equatorial ionosphere-thermosphere (I–T) coupling system.

The physics behind EEJ is the horizontal geomagnetic field geometry, which can bind the conducting ionospheric E region from the atmosphere below and less-conducting F region above. Previous studies have suggested that the primary driver of EEJ is the large-scale ionospheric daytime eastward electric field in the E region (Heelis, 2004). The vertical Hall current at the dip equator can be triggered for the eastward electric field, accumulating positively and negatively charged particles at the upper and lower boundaries, respectively. Charged particles at the boundaries can result in an additional radial polarization electric field, thus, significantly enhancing the prevailing Pedersen conductivity. The combined effect of Hall and Pedersen conductivities, termed as Cowling conductivity, leads to the intense currents in the east–west direction at the daytime dip equator. However, the typical daytime eastward electric field can sometimes reverse, resulting in westward intense currents, which have been discovered by Gouin (1962) and termed as CEJ by Gouin and Mayaud (1967).

The temporal signals of EEJ and CEJ during geomagnetic storms have been reported previously (Kikuchi et al., 2000, 2003; Yamazaki & Kosch, 2015; Yizengaw et al., 2011). Using ground-based equatorial magnetometer data, Yizengaw et al. (2011) disclosed that $E \times B$ drifts under CEJ conditions are stronger in the American sector and 16 UT than in the African sector and 06 UT at the same local time. Using long-term records of magnetometer data from the Indian and Peruvian stations, Yamazaki and Kosch (2015) investigated the climatology of EEJ during geomagnetic storms. They found that during a similar magnitude of geomagnetic and solar EUV activities, the peak intensity of disturbance noon EEJ in June was stronger at 75° W GLon and 17 UT (−16 nT) than at 75° E GLon and 07 UT (−9 nT). Previous studies have mainly focused on the intensity and direction variations in EEJ during storm time, which has been divided into two periods, the main and recovery phases. During a storm, the intensity and polarity of EEJ are influenced by the prompt penetration electric field (PPEF) and disturbance dynamo electric field (DDEF; Bulusu et al., 2018; Kikuchi et al., 2008; Wang et al., 2019; Yamazaki & Kosch., 2015; Zheng et al., 2018). The main difference between the effects of PPEF and DDEF on EEJ is the time scale. EEJ associated with PPEF typically varies within a few hours (Manoj et al., 2008), whereas EEJ due to DDEF develops more slowly and can last for several hours to days owing to the inertia of neutral air (Huang et al., 2005). Based on the CHAMP-observed scalar magnetic field data, Zheng et al. (2018) explored the characteristics of temporal variations in EEJ during two storm events on 15 May and 24 August 2005. The results showed that PPEF associated with the imbalance between Region 1 field-aligned currents (FACs) and Region 2 FACs was responsible for the enhancement of eastward EEJ during the main phase whereas the peak of westward EEJ during the recovery phase coincided in time and space with the equatorward penetration of atmospheric mass density, indicating the important effects of meridional wind. The westward EEJ can be caused by R2 FACs during recovery phase, which were confirmed by previous studies (e.g., Kikuchi et al., 2008). However, the roles of R2 FACs cannot be investigated by using the ionosphere-thermosphere model TIEGCM without the ring current processes involved. The detailed analysis of the role of R2 FACs in the EEJ might be left in the future by using magnetosphere-ionosphere coupling model (i.e., coupled magnetosphere ionosphere thermosphere model, CMIT). We think such discrepancy might be one of the causes for the model-observation discrepancy. Using ground-based daytime magnetic field data, Bulusu et al. (2018) studied the effects of ionospheric electric field on EEJ, and they found that the physical processes of PPEF and DDEF compete with each other, and both of them play critical roles in EEJ disturbance. However, the temporal variations in residual EEJ throughout the day due to subauroral polarization streams (SAPS) have not been investigated previously.

SAPS is an interesting physical phenomenon that is an intense westward plasma flow at subauroral latitudes, and the main characteristics of SAPS are as follows: a latitudinally narrow region spanning from 3° to 5° at an amplitude of greater than hundreds of m/s and extending from pre-midnight to afternoon sector along subauroral latitudes (Foster & Vo, 2002). Previous studies have reported variabilities in the equatorial I–T system during SAPS period (Aa et al., 2021; Ebihara et al., 2014; Huang, 2020; Wang et al., 2008, 2019; Zhang, Wang, et al., 2021). For example, using FPI observations and TIEGCM simulations, Zhang, Wang, et al. (2021) explored the UT variations in SAPS-induced northward wind at night-time and mid-latitudes. The results indicated that the poleward wind shows significant UT variations due to misalignment between geographic and geomagnetic coordinates. The disturbance wind owing to SAPS could travel to the dip equator and establish a zonal electric field via wind dynamo, introducing possible disturbances in EEJ. During a minor but quite geo-effective storm on 27–28 September 2019, Aa et al. (2021) found that the large-scale traveling ionospheric disturbances (TIDs) generated during the main phase can be significantly modulated by SAPS. The large-scale TID related to SAPS could travel to the dip equator, producing potential EEJ changes. Based on 10 years of CHAMP observations, Wang et al. (2019) found that CEJ occurrence during SAPS periods doubles as compared to normal periods, suggesting the potential effects of SAPS. However, temporal differences in disturbance EEJ due to SAPS have seldom been investigated. Understanding the response of daytime EEJ to SAPS is important. As SAPS is a common feature during storm times, EEJ is key in understanding equatorial electrodynamic and has a significant influence on human activities, that is, communication technology and metallic conduct networks. This study aims to disclose the temporal responses of EEJ to SAPS and determine the potential physical drivers, which can help the understanding of SAPS effects on the high–low latitude coupling of upper atmosphere and coupling between the ionosphere and thermosphere at dip equator.

For the completeness of this work, two simulations with and without SAPS ion velocity imposed in TIEGCM were performed to identify the roles of SAPS. By adopting a similar approach as Wang et al. (2012), the SAPS ion velocity is imposed into the subauroral region in the TIEGCM, with the location and magnitude determined

Table 1
Locations of Equatorial and Off-Equatorial Stations

Stations (code)		GLon	GLat	MLat
Equatorial	Tirunelveli (TIR)	77.8°E	8.7°N	0.8°N
	Addis Ababa (AAE)	38.77°E	9.03°N	0.17°N
	Mbour (MBO)	17°W	14.38°N	0.11°N
Off-equatorial	Alibag (ABG)	72.9°E	18.6°N	11.9°N
	Ethiopia (ETHI)	39.46°E	14.28°N	5.9°N
	Ascension Island (ASC)	14.4°W	7.95°S	9.74°S

by the 3-hr Kp index. In ground- and space-based measurements, we investigated the temporal variations in SAPS velocity, EEJ, and associated vertical $E \times B$ drifts, ensuring the reliability and stability of models in capturing the temporal signals of SAPS and EEJ. To explore the possible mechanisms that play important roles in the temporal variations of SAPS-induced residual EEJ (ΔEEJ), the contributions from PPEF and DDEF were distinguished in TIEGCM. A similar method was applied to the study of zonal and meridional wind effects. The layout of this paper is as follows: data and model descriptions are included in Section 2, data-model comparisons are described in Section 3, possible physical mechanisms for the temporal structure of ΔEEJ are explored in Section 4, and the findings of this work are summarized in Section 5.

2. Data and Model

The SAPS events are identified by the observational cross-track ion velocity from the Defense Meteorological Satellite Program (DMSP). The EEJ data are obtained by processing the hourly averaged horizontal geomagnetic field data, and the equatorial and off-equatorial stations are listed in Table 1. The SAPS selection and EEJ processing have been described in detail in our first paper (Zhang, Yamazaki, et al., 2021, under review). The EEJ and vertical $E \times B$ observations from AAE and Jicamarca stations have been obtained from AMBER and SAMBA networks (Yizengaw & Moldwin, 2009). The Communications/Navigation Outage Forecasting System (C/NOFS) was developed by the Air Force Research Laboratory Space Vehicles Directorate to investigate and forecast scintillations in the Earth's ionosphere (de La Beaujardière and The C/NOFS Definition Team, 2004). It was launched on 16 April 2008 with a low Earth orbit and an orbital inclination of 13°. The measured vertical $E \times B$ drifts were used in this study to determine the reliability of the model in reproducing EEJ and vertical plasma drifts. The detail description of TIEGCM model and the method to distinguish the effects of DDEF owing to total, zonal, and meridional winds are also given in our first paper (Zhang, Yamazaki, et al., 2021, under review).

3. Results

3.1. Geomagnetic Conditions

Figure 1 shows the temporal variations in Dst and Kp indices during a moderate geomagnetic storm on 1 June 2013. In Figure 1a, the Dst index rapidly decreases from 13 nT at storm time 00 hr to -124 nT at storm time 09 hr, indicating the main phase of geomagnetic storm. In the rest of the paper, the storm time is simplified: for instance, "at storm time 00 hr" is simplified to "at 00 hr." Note here that the storm time 00 hr corresponds to 00 UT. Following this, the Dst index slowly increases to -44 nT at 24 hr, indicating the recovery phase. At 12–14 hr, the Dst index maintained a similar magnitude of -83 nT. Therefore, in this case, both the main and recovery phases of the storm were covered. On June 01, the Kp index (Figure 1b) was 5.7 at 00–03 hr; it then achieved a maximum value of 7 at 03–06 hr, indicating the strongest disturbances. At 06–12 hr, the Kp index decreased from 6.3 to 4.7. At 12–15 hr, the Kp index showed a second peak of 5.7. Subsequently, the Kp index rapidly decreased to approximately 3, and it maintained similar strength at 15–24 hr. The Kp index has been shown in the current work because the empirical SAPS model is determined by the Kp index. Therefore, the SAPS velocity should have a high degree of similarity with the large-scale patterns of Kp index, that is, increasing from 00 to 06 hr, achieving the maximum at ~ 06 hr, then slowly decreasing to 24 hr with a secondary peak at ~ 15 hr, which will be proved later in DMSP observations (Figure 2b) and TIEGCM simulations (Figure 2c).

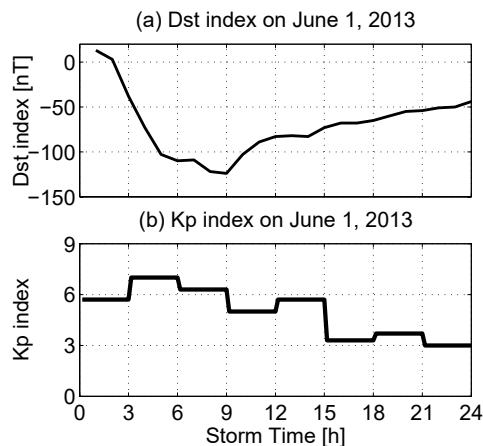


Figure 1. The temporal variations in Dst (top) and Kp (bottom) indices on 01 June 2013.

Figure 2a shows an example of a SAPS event based on the observed ion velocity from the DMSP F16 satellite on 1 June 2013. The quiet-time ion

3.2. SAPS Reproduction

Figure 2a shows an example of a SAPS event based on the observed ion velocity from the DMSP F16 satellite on 1 June 2013. The quiet-time ion

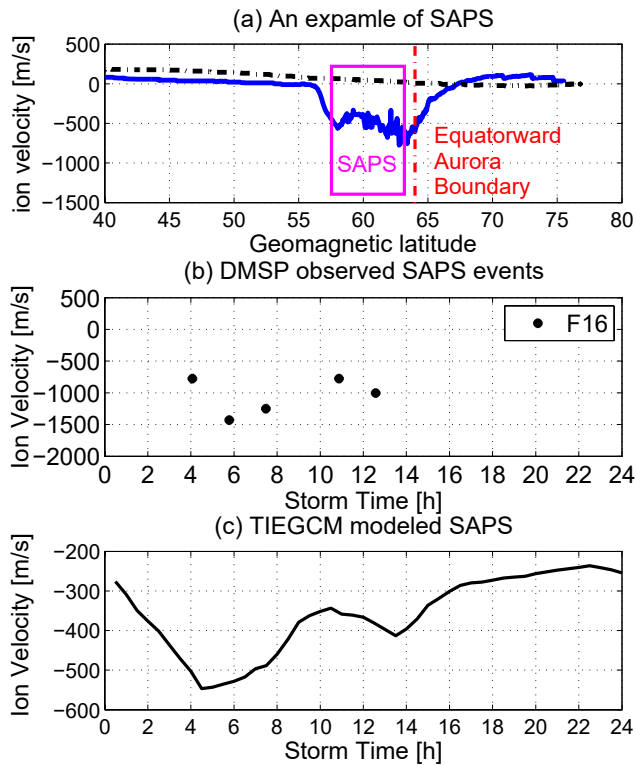


Figure 2. (a) An example of the subauroral polarization streams (SAPS) event on 1 June 2013, based on the defense meteorological satellite program (DMSF) F16-observed ion velocity (blue line). The black line is the observed ion velocity without SAPS event on 31 May 2013. (b) The DMSF F16 observed SAPS on 1 June 2013. (c) The temporal variations of thermosphere-ionosphere electrodynamic general circulation model (TIEGCM)-SAPS modeled SAPS velocity at ~ 400 km.

velocity was eastward at the middle and high latitudes, and it ranged from 100 to 200 m/s. Contrary to the quiet-time ion velocity, a significantly strong westward flow occurred at a narrow latitudinal region of 57° – 63° MLat, with a velocity of approximately -500 m/s. Note here that the positive value stands for eastward flow. This is a well-known SAPS, indicated by the magenta square and text. The observed SAPS event was located at the equator side of aurora, in agreement with previous studies (Foster & Vo, 2002). Figure 2b shows the temporal variations of observed SAPS velocity at 15–17 MLT from DMSF F16 on 1 June 2013. Five SAPS events were also observed, and their corresponding SAPS velocities were -776 m/s at 04 hr, $-1,429$ m/s at ~ 06 hr, $-1,250$ m/s at ~ 07 hr, -775 m/s at 11 hr, and $-1,005$ m/s at ~ 13 hr. Figure 2c shows the temporal variations in the TIEGCM-SAPS modeled SAPS velocity. The SAPS velocity yielded a pattern similar to the letter “W,” decreasing from approximately -300 m/s at 00 hr to -543 m/s at 05 hr, slowly increasing to -343.6 m/s at ~ 11 hr, then decreasing to -413 m/s at ~ 14 hr, and increasing slowly to -250 m/s at 24 hr. A comparison between Figures 2b and 2c shows that a similar large-scale pattern of SAPS velocity was reproduced in TIEGCM-SAPS, indicating its reliability in capturing SAPS. However, SAPS velocity was underestimated in the model, which might be caused by two factors. First, it might be related to the empirical SAPS model, which was developed from the statistical results. Second, it may be a result of the high-latitude electric field driver of Heelis empirical model (Heelis et al., 1982), which predicts the average state of high-latitude ion convection for a given 3-hr Kp index. The real high-latitude electric field varies rapidly with time, and it cannot be captured to a perfect degree in the model. However, data-model discrepancy is acceptable in model work due to a high degree of similarity in the temporal variations of SAPS velocity (Figures 2b–2c). TIEGCM has been used to explore the effects of SAPS on the global I–T system, and a good agreement between model outputs and observations has been achieved in previous studies (Wang et al., 2012, 2019; Zhang, Wang, et al., 2021). Both the large-scale patterns of modeled and observed SAPS velocities were inversely proportional to those of Kp index (Figure 1b). As the SAPS flows westward and is negative in the measurements. Therefore, the strongest SAPS (trough) corresponds to the strongest Kp (peak), further confirming the reliability of the model.

3.3. Data-Model Comparison

Figure 3a shows the temporal distributions of noon EEJ from ground-based measurements and TIEGCM simulations. The TIEGCM-default modeled EEJ (black line) showed three peaks and troughs. The three peaks were located at 04, 12, and 18 hr, with intensities of 24.3, 14.6, and 18.1 mA/m, respectively. Three troughs occurred at 08, 15, and 24 hr with magnitudes of 12.9, 4.8, and 5.4 mA/m, respectively. A similar large-scale temporal structure was observed in TIEGCM-SAPS results; however, the intensities of both peaks and troughs were much weaker than those from TIEGCM-default. The peaks had values of 19.0, 10.48, and 13.9 mA/m, respectively, and the troughs had intensities of 5.5, -1.5 , and 1.6 mA/m, respectively. In comparison with TIEGCM-default results, the magnitude of TIEGCM-SAPS modeled noon EEJ was more similar to the ground-based observations. Because at 07 (TIR), 09 (AAE), and 13 hr (MBO), the average observed EEJ had an intensity of 3.8, 3.7, and -11.2 mA/m whereas the modeled noon EEJ from TIEGCM-SAPS (TIEGCM-default) had an intensity of 7.0 (14.67), 7.1 (13.29), and 6.8 (11.1) mA/m, respectively. Note here that both the observed and modeled EEJ are significantly decreased from storm time 09–13 hr, indicating the qualitatively reproducing temporal changes, hence the reasonable of the data-model discrepancy at storm time 13 hr. Thus, TIEGCM-SAPS performs better in reproducing the temporal patterns of EEJ during storms. Therefore, SAPS effects play a critical role in the temporal variations of EEJ, and they should be explored. The data-model discrepancy is acceptable in model work owing to the similar temporal variations of EEJ reproduced in the model. Furthermore, the ground-observed noon

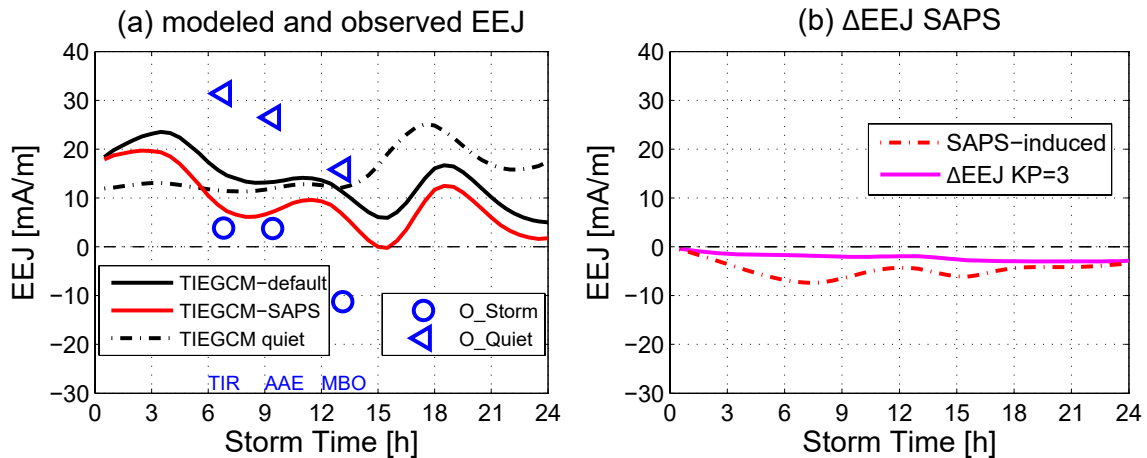


Figure 3. (a) The temporal variations of ground observed (blue circle for storm time, blue triangle for quiet time), Thermosphere-Ionosphere Electrodynamic General Circulation Model (TIEGCM)-default (black solid line), and TIEGCM-SAPS (red solid line) modeled noon equatorialelectrojet (EEJ) at 01 June 2013. The black dotted line is the quiet-time EEJ from TIEGCM-default at May 31. The EEJ is given in mA/m. (b) Similar to Figure 3a, but for modeled SAPS-related Δ EEJ (red dotted line). The SAPS-related Δ EEJ is the differences between TIEGCM-SAPS and TIEGCM-default. The magenta line is the SAPS-induced Δ EEJ when Kp equals 3.

EEJ at three stations during storm (O_storm, 01 June 2013) and previous quiet time (O_quiet, 31 May 2013) are shown in blue circle and triangle in Figure 3a, respectively. It can be found that EEJ is significantly enhanced in the westward direction, from an average value of 20–30 mA/m to an average value of -10 – 5 mA/m. This westward shift can be caused by the combined effects of SAPS and geomagnetic activity.

Figure 4a shows the observed vertical $E \times B$ drifts from Jicamarca and AAE stations and C/NOFS satellite and simulations from the two models. The C/NOFS observed equatorial vertical $E \times B$ drifts have speeds of -5 – 0 and 5 – 15 m/s at 15 and 21 hr, respectively. The corresponding TIEGCM-SAPS (TIEGCM-default) modeled vertical $E \times B$ drifts were 0.9 (6.6) and 7.3 (12.2) m/s, respectively. The average observed $E \times B$ drifts at Jicamarca and AAE stations were 12.63 and 2.13 m/s, respectively. The corresponding TIEGCM-SAPS (TIEGCM-default) modeled $E \times B$ drifts were 8.16 (12.51) and 8.5 (14.9) m/s, respectively. Therefore, in comparison with these observations, the $E \times B$ drifts from both models had a similar temporal variation, confirming the reliability of these models. Moreover, as compared to vertical $E \times B$ drifts from TIEGCM-default, the results from TIEGCM-SAPS were more similar to the observations. This indicates that TIEGCM-SAPS works better than TIEGCM-default in

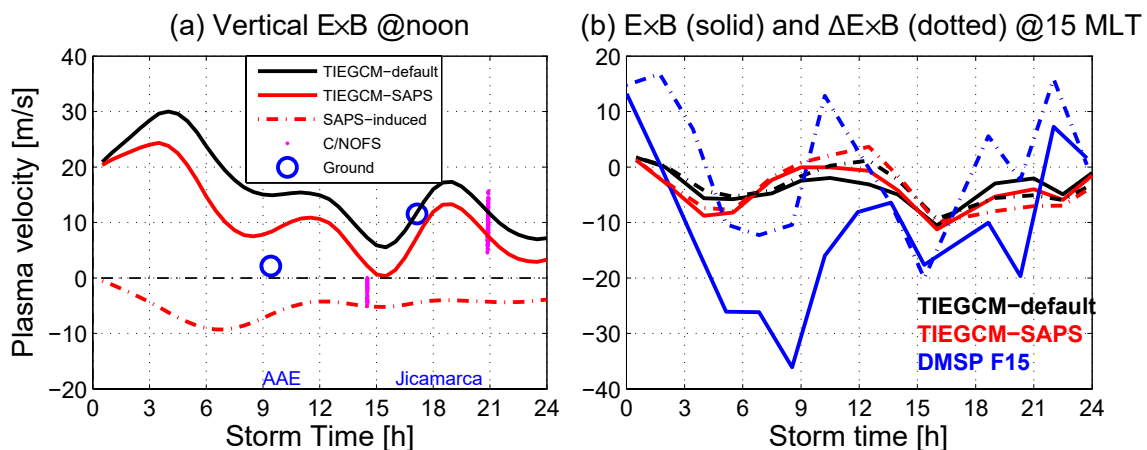


Figure 4. (a) The temporal variations of communications/navigation outage forecasting system (C/NOFS) (magenta dots) and ground observed (blue circle), thermosphere-ionosphere electrodynamic general circulation model (TIEGCM)-default (black solid line), and TIEGCM-SAPS (red solid line) modeled vertical $E \times B$ drift at 180 km. The vertical $E \times B$ drifts are given in m/s. The positive value stands for the upward $E \times B$. (b) The temporal variations of observed and modeled vertical plasma velocity (WI, solid line) and the residual WI (Δ WI, dotted line) at 01 June 2013. The Δ WI is obtained by removing the quiet time WI (31 May 2013) from storm time WI. The blue, black, and red lines are DMSP F15 observations, TIEGCM-default and TIEGCM-SAPS simulations, respectively.

capturing vertical $E \times B$ drifts, and the SAPS effects were critical in the reproduction of temporal variations of vertical $E \times B$ drifts at the dip equator. The good reproduction in vertical $E \times B$ indicates a good definition of the ionospheric zonal electric field, EEJ. To well confirm the reliability of model, a comparison between observed and modeled equatorial vertical plasma velocity (WI, solid line) and residual WI (Δ WI, dotted line) during storm time (June 01) is shown in Figure 4b. The reason why data from DMSP F15 is selected here is that the MLT of DMSP F15 is 15 MLT, which is closest to noon among all four DMSP satellites (F15–F18). It can be found that WI decreases from ~ 12 m/s at 00 hr to -35 m/s at 08 hr, increases to -8 m/s at 13 hr, then decreases to -20 m/s at 16 hr, and finally smoothly increases to around 0 m/s at 24 hr, yielding a pattern similar to the letter “W.” A similar large-scale temporal structure is found in TIEGCM-SAPS and TIEGCM-default simulations but with differences in the speed. The real geomagnetic activity rapidly changes with time, potentially causing differences between model predictions and satellite observations. The same patterns are found in the modeled and observed Δ WI, indicating the reliability of model in capturing the temporal variations.

The red dotted line in Figure 3b is the SAPS-induced noon Δ EEJ, which is the difference between the modeled EEJ from TIEGCM-SAPS and TIEGCM-default. When small-scale fluctuations are ignored, the SAPS-induced Δ EEJ yields an obvious temporal structure similar to the letter “W,” which is different from the modeled noon EEJ. Note that this temporal structure actually shows the mixture of temporal and longitude variations of SAPS-induced Δ EEJ. To show the longitudinal differences, a case with Kp index of 3 has been performed in both TIEGCM-SAPS and TIEGCM-default, with their differences indicating by the magenta line in Figure 3b. The result in magenta line indicates that there has an accumulation of SAPS effects with respect to time, and does not show great longitudinal dependence. Thus, the result in Figure 3b (red dotted line) is purely temporal variations, which is our focus. The SAPS-induced Δ EEJ mainly flows westward, that is, CEJ. SAPS-induced CEJ rapidly enhanced westward from 00 mA/m at 00 hr to -7.5 mA/m at 07 hr, then decreased slowly to -4.0 mA/m at 12 hr, enhanced westward to -6.5 mA/m at 15 hr, and then decreased slowly to -3.4 mA/m at 24 hr. A comparison between Figures 3b and 2c shows that the large-scale trend of SAPS-induced CEJ had a large degree of similarity to that of SAPS velocity but with a time delay of 2–3 hr, indicating a proportional relationship between the two, that is, faster the SAPS, stronger the intensity of CEJ 2–3 hr later. However, the primary drivers of temporal distribution of SAPS-induced CEJ are still poorly understood. The cause of time delay is still unknown, which might account for the traveling disturbances from high latitudes to the dip equator, and it will be explored later. Furthermore, the temporal variations of SAPS-driven Δ EEJ might contain variations in the ionospheric electric field and Cowling conductivity. As disclosed in Zhang, Yamazaki, et al. (2021), the relative changes in the Cowling conductivity due to SAPS are much weaker than that in the electric field. Thus, only the effects of electric field are left in the temporal variations of SAPS-induced Δ EEJ. The red dotted line in Figure 4a is the SAPS-induced vertical $E \times B$ drifts ($\Delta E \times B$), which is also the difference between TIEGCM-SAPS and TIEGCM-default. The temporal variations of $\Delta E \times B$ also form an obvious structure similar to the letter “W,” that is, two troughs of -9.5 m/s at 07 hr and -5.4 m/s at 15 hr and one peak of -4 m/s at 12 hr. The temporal variations of $\Delta E \times B$ drifts were the same as those of SAPS-induced CEJ. A positive value indicates an upward $E \times B$. The downward $\Delta E \times B$ represents the westward electric field owing to SAPS.

4. Discussion

4.1. Time Delay

A comparison between Figures 3b and 2c reveals a time delay of 2–3 hr between the temporal variations of CEJ and SAPS velocity. To determine the potential drivers, we should first identify the physical mechanisms involved in the modulation of Δ EEJ during the SAPS period. Previous studies have disclosed that EEJ is controlled by two factors, ionospheric conductivity and zonal electric field (Lühr et al., 2008; Yamazaki & Maute, 2017). The intense current (J_E) at dip equator can be expressed as $J_E = \left(\sigma_P \frac{\sigma_H}{\sigma_P} \right) E$, where σ_P , σ_H , and $\sigma_P + \frac{\sigma_H}{\sigma_P}$ are the Pedersen, Hall, and Cowling conductivities, respectively (Yamazaki & Maute, 2017). The daytime ionospheric zonal electric field (E) at EEJ altitudes was generally eastward at the dip equator, and it reversed sometimes. Thus, the temporal variations of Δ EEJ can be determined using the changes in ionospheric cowling conductivity (Δ Cowling) and zonal electric field (Δ Zonal E), as shown in Figure 5. In Figure 5a, Δ Zonal E rapidly enhanced westward from -0.1 at 00 hr to the trough value of -0.38 mV/m at 07 hr. Although the zonal electric field is enhanced in westward for the SAPS effects, the daytime eastward penetration electric field during main phase is observed by Jicamarca incoherent scatter radar and EEJ (Kikuchi et al., 2008). After 07 hr, the westward Δ Zonal E slowly gets

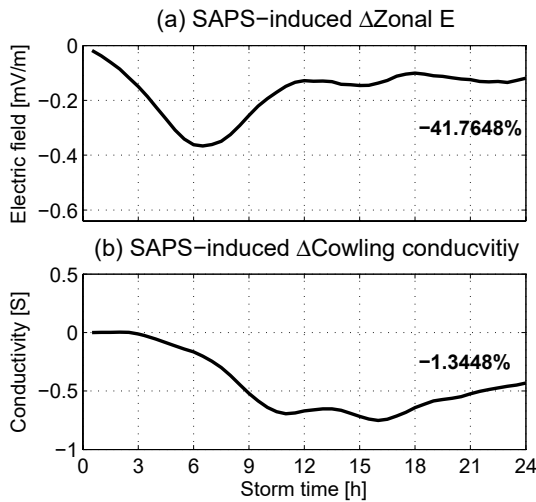


Figure 5. The temporal variations in the subauroral polarization streams (SAPS)-induced (a) $\Delta Zonal E$ and (b) $\Delta Cowling$. The $\Delta Zonal E$ and $\Delta Cowling$ are given in mV/m and S, respectively. The mean changes in percentage are given in black bold at right side.

on ΔEEJ . The PPEF-induced ΔEEJ varies within a few hours (Manoj et al., 2008) whereas DDEF-induced ΔEEJ develops more slowly and can last for several hours to days owing to the inertia of neutral air (Huang et al., 2005). However, this key factor may not be suitable for our study. The SAPS effects are imposed on the global ionosphere-thermosphere system throughout the day. The effects of PPEF and DDEF generated by SAPS lasted for 24 hr. A question posed here is whether PPEF, DDEF, or both dominate the time delay. However, as shown in Figure 6a, both $\Delta Zonal E$ and CEJ associated with PPEF are negligible (almost 0), and they have no significant temporal variations, thus, indicating the negligible role of PPEF. Because by adopting a similar approach as Wang et al. (2012), the SAPS ion velocity is imposed into the subauroral region at all altitudes in the TIEGCM, with the location and magnitude determined by the 3-hr Kp index. In our simulation, the background $E \times B$ drift at subauroral region has been replaced by the imposed SAPS ion velocity, for emphasizing the SAPS induced effects into the Ionosphere-Thermosphere system. Since the SAPS is included after the calculation of the electric potential, it will not directly affect the equatorial electric fields. In other words, at low latitudes, there is no PPEF generated by SAPS but only PPEF from the Heelis model. Nonetheless, the effect of DDEF by SAPS can be reproduced, as the Joule heating is calculated using ion velocities.

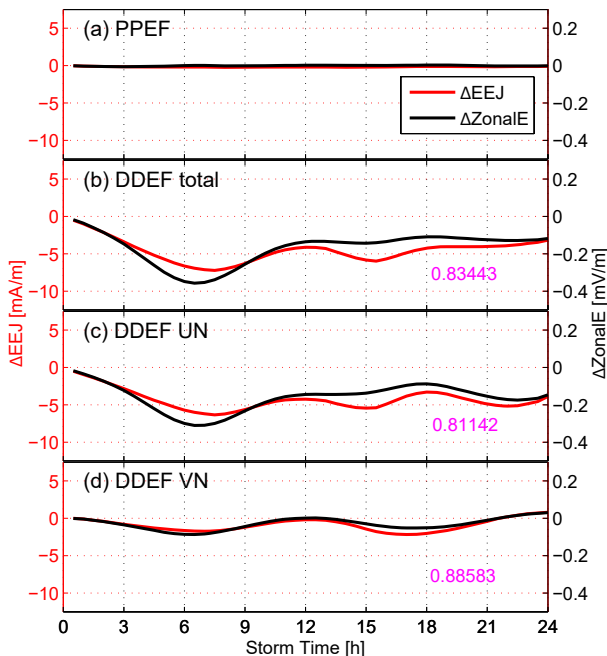


Figure 6. The temporal variations in ΔEEJ (red) and $\Delta Zonal E$ (black) due to (a) prompt penetration electric field (PPEF), (b)–(d) disturbance dynamo electric field (DDEF) owing to total wind, zonal wind (UN), and the meridional wind (VN), respectively. The correlate coefficient is given in magenta color at the upper right.

decreased to -0.1 mV/m, with a secondary trough of -0.15 mV/m at 15 hr. The same temporal variations occur in both $\Delta Zonal E$ and CEJ, suggesting that the temporal variations of ΔEEJ might be attributed to $\Delta Zonal E$. To evaluate this assumption, Figure 5b shows the temporal variations of $\Delta Cowling$. $\Delta Cowling$ does not exhibit similar temporal variations with ΔEEJ , indicating a minor contribution to ΔEEJ . Additionally, the mean changes of $\Delta Zonal E$ in percentage are -41.76% , which is tens of the relative changes in $\Delta Cowling$ (-1.34%). These results further support our conclusion that the time delay of ΔEEJ is mainly driven by $\Delta Zonal E$, with negligible roles of $\Delta Cowling$. This result seems to disagree with Jadhav et al. (2002) and Yamazaki et al. (2017), who highlighted the important effects of ionospheric conductivity in the longitudinal distributions of EEJ. In our study, the temporal structures of CEJ were studied during SAPS periods whereas previous studies focused on the quiet-time value.

A good agreement was observed between the temporal variations of $\Delta Zonal E$ (Figure 5a) and SAPS velocity (Figure 2c), but with a time delay of 2–3 hr, that is, faster the SAPS speed, larger the $\Delta Zonal E$ at 2–3 hr later. Therefore, 2–3 hr is the cost for the SAPS effects to establish enough $\Delta Zonal E$ to affect CEJ. $\Delta Zonal E$ can be separated into two components, namely PPEF and DDEF (Bulusu et al., 2018; Huang et al., 2005; Manoj et al., 2008; Wang et al., 2019; Yamazaki & Kosch, 2015). Previous studies have reported that time scale was the critical factor for separating the effects of PPEF and DDEF

Figure 6b shows the temporal variations of $\Delta Zonal E$ and CEJ associated with DDEF owing to total wind. In comparison with $\Delta Zonal E$ in Figure 5a (ΔEEJ in Figure 3b), $\Delta Zonal E$ (ΔEEJ) associated with DDEF owing to total wind has comparable magnitudes and similar structures. This supports our conclusion that SAPS-induced $\Delta Zonal E$ and CEJ mainly account for the effects of DDEF. Additionally, the coefficient between $\Delta Zonal E$ and CEJ in Figure 6b was 0.83443, confirming the critical role of $\Delta Zonal E$ due to DDEF. The DDEF effects can be separated into two components: zonal and meridional wind, which have been proposed to explain storm-time EEJ (Anandarao & Raghavarao, 1987; Wang et al., 2019; Zheng et al., 2018). The thermospheric zonal and meridional winds can establish the zonal electric field through wind dynamo (Blanc & Richmond, 1980) and then drive EEJ.

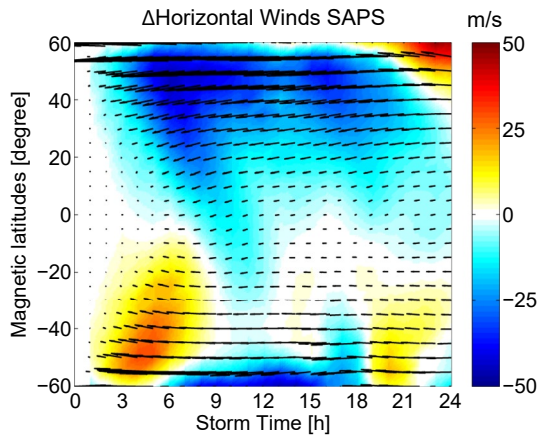


Figure 7. The storm time and geographic latitude variations of subauroral polarization streams (SAPS)-induced disturbance meridional winds (color) and horizontal winds (arrows) at noon at 180 km.

In Figure 6c, the temporal changes in Δ Zonal E from DDEF owing to zonal wind have a large degree of similarity with Δ Zonal E in Figure 5a (total Δ Zonal E) and 6b (Δ Zonal E owing to total DDEF) because both have a comparable value ranging from -0.1 to -0.4 mV/m and have similar temporal structure in letter “W.” Additionally, the coefficient between Δ Zonal E and CEJ in Figure 6c was 0.81142. This suggests that the time delay between SAPS-induced CEJ and SAPS velocity might be related to the disturbance zonal wind that travels from subauroral latitudes to the dip equator in 2–3 hr (Fujiwara & Miyoshi, 2006; Zhang et al., 2019).

To evaluate this conclusion, Figure 7 shows the storm-time evolution of SAPS-induced disturbance horizontal and meridional winds at noon at an altitude of 180 km. The SAPS-induced CEJ at 00–03 hr might be related to the dynamo action of mid-latitude wind surges (Fuller-Rowell et al., 2002; Zheng et al., 2018). The westward disturbance wind at mid-latitudes drives equatorward currents, leading to a build-up of positive charges at lower latitudes, thus a poleward electric field. Note that the equatorward currents are canceled out by poleward Pedersen currents owing to the poleward electric field. The poleward electric field can also produce eastward Hall currents, leading to a build-up of positive charges at dusk terminator, generating a

westward electric field at lower latitudes that leaks to the equator, hence CEJ. At 03–24 hr, the disturbance wind arrives low latitudes and flows westward at the dip equator with a speed of several m/s. The phase speed of traveling atmospheric disturbances in SAPS-induced meridional wind is ~ 600 m/s, consistent with previous studies (i.e., Bruinsma & Forbes, 2007; Zhang et al., 2019). At 03–24 hr, the equatorial local disturbance wind in westward produces a westward electric field, hence CEJ. In summary, SAPS-related disturbance wind travels to the dip equator in 2–3 hr, causing the time delay between CEJ and SAPS.

4.2. Roles of Meridional Wind

Previous studies have disclosed that both the zonal and meridional winds can play a role in zonal electric field, causing EEJ changes (Anandarao & Raghavarao, 1987; Wang et al., 2019; Zheng et al., 2018). As previously discussed, the temporal variations of SAPS-induced CEJ and time delay with respect to SAPS are mainly controlled by DDEF owing to the zonal wind. However, the temporal variations of CEJ and Δ Zonal E due to meridional wind (Figure 6d) cannot be ignored, which have a maximum value of -2.3 mA/m and -0.1 mV/m, respectively. Additionally, the coefficient between Δ Zonal E and CEJ in Figure 6d was 0.88583. It can be concluded that the meridional wind can modulate CEJ as much as an average percentage of 16% via wind dynamo. In the SAPS channel, the neutrals were driven westward by a strong westward ion flow. Because of the ion-neutral interaction, that is, frictional heating, significant temperature changes are produced (Wang et al., 2012). Owing to the misalignment between geomagnetic and geographic fields, the westward ion drag effects would project into the geographic meridian, driving the geographic meridional wind (Zhang, Wang, et al., 2021). Due to global circulation, the disturbance wind would extend to lower latitudes, wider local times, and longitudes. The generated zonal and meridional winds are proportional to SAPS strength. Stronger the SAPS velocity, faster the disturbance wind (Figure 7). Thus, the equatorial meridional wind associated with SAPS should also be proportional to SAPS strength with a time delay of 2–3 hr, which is the time cost of atmospheric disturbances traveling from the SAPS channel to dip equator. The stronger meridional wind should expectedly produce a stronger zonal polarization electric field, resulting in a strong CEJ. However, the temporal structures of CEJ and Δ Zonal E owing to meridional wind (red and black lines in Figure 6d) were significantly different from SAPS velocity. It has a structure similar to the sine function, that is, two troughs at 07 and 16 hr and three peaks at 00, 12, and 24 hr. The peaks represent the weakest CEJ and westward Δ Zonal E . The potential drivers for unexpected structures are still unknown, and they should be explored.

Collisional interactions between neutrals and plasma at the E-layer can produce ionospheric currents and electric field, which can be expressed as $J = \sigma \cdot (E + U \times B)$, where σ , E , U , and B are the ionospheric conductivity, electric field, neutral wind, and ambient magnetic field, respectively (Blanc & Richmond, 1980; Yamazaki et al., 2021). The ionospheric zonal current and electric field due to meridional winds (VN) can be expressed by

$VN \cdot \sin D \cdot B$, where D is the declination and B is the magnetic field strength. Note here that $VN \cdot \sin D$ is the geomagnetic zonal component of southward geographic wind. Therefore, the equatorward winds could produce eastward currents. At dip equator, no changes in EEJ could be caused by the local meridional winds because the local magnetic field and meridional winds are in the same direction (Yamazaki et al., 2021). However, the disturbance meridional winds at mid-latitudes are effective in modulating the EEJ during storm time. The positive charges at dusk terminator could be built up because of the generation of eastward currents owing to the equatorward winds at mid-latitudes (Figure 7). Then, a westward electric field is produced at lower latitudes, causing westward Δ EEJ as shown in Figure 6d. In Figure 7, the equatorward winds at mid-latitudes are significantly stronger at 07 and 16 hr than that at 12 and 24 hr. Therefore, CEJ and westward Δ Zonal E (Figure 6d) due to SAPS-generated equatorward winds were significantly enhanced (reduced) at 07 and 16 hr (12 and 24 hr) as compared to other storm times.

5. Conclusions

Using ground-based magnetic field observations and numerical simulations from TIEGCM-default and TIEGCM-SAPS, the temporal variations of SAPS-induced noon Δ EEJ were investigated in this study. Several interesting results were obtained.

1. The temporal variations of SAPS-excited noon CEJ were almost the same as SAPS velocity, which was determined by the Kp index. Larger the Kp , faster the SAPS velocity and stronger the noon CEJ. However, there was a significant time delay of 2–3 hr between noon CEJ and SAPS
2. The primary driver of temporal variations was the electric field changes owing to the disturbance dynamo electric field from the zonal wind. Stronger the SAPS velocity, faster the disturbance wind. The ionospheric Cowling conductivity played a negligible role in the modulation of EEJ. As the Cowling conductivity does not agree well with the SAPS-related CEJ
3. The time delay of 2–3 hr is a result of the traveling atmospheric disturbances from high to low latitudes. The SAPS-generated zonal and meridional wind at high latitudes could extend to the dip equator in 2–3 hr, producing the corresponding westward electric field to excite CEJ
4. The temporal variations of CEJ and westward Δ Zonal E owing to meridional wind accounted for 16%. The storm-time disturbance equatorward winds at mid-latitudes could lead to the accumulation of positive charges at dusk terminator owing to the generation of eastward currents. Consequently, a westward electric field could be established at lower latitudes, changing EEJ

Data Availability Statement

The simulation data are stored in Zenodo (https://zenodo.org/record/4895729#.YLg6p_kzaUk). The ground-based magnetometer data are available on the website (<http://wdciig.res.in/WebUI/MinData.aspx>). The DMSP data are available in the madrigal hosted by CEDAR (<http://cedar.openmadrigal.org/>).

Acknowledgments

The National Center for Atmospheric Research is sponsored by the National Science Foundation. We are grateful for the sponsor from the Fundamental Research Funds for the Central Universities (2042021kf0208), the National Nature Science Foundation of China (No. 41974182, 41674153, and 42004135), and China Postdoctoral Science Foundation (2020M682465). The authors thank E. Yizengaw, E. Zesta, M. B. Moldwin, and the rest of the AMBER and SAMBA team for the data (<http://magnetometers.bc.edu/index.php/downloads>). AMBER is operated by Boston College and funded by NASA and AFOSR. SAMBA is also operated by UCLA and funded by NSF.

References

- Aa, E., Zhang, S. R., Erickson, P. J., Coster, A. J., Goncharenko, L. P., Varney, R. H., & Eastes, R. (2021). Salient midlatitude ionosphere-thermosphere disturbances associated with SAPS during a minor but geo-effective storm at deep solar minimum. *Journal of Geophysical Research: Space Physics*, 126(7), e2021JA029509.
- Alken, P., & Maus, S. (2010). Relationship between the ionospheric eastward electric field and the equatorial electrojet. *Geophysical Research Letters*, 37, L04104. <https://doi.org/10.1029/2009GL041989>
- Anandarao, B. G., & Raghavarao, R. (1987). Structural changes in the currents and fields of the equatorial electrojet due to zonal and meridional winds. *Journal of Geophysical Research*, 92(A3), 2514. <https://doi.org/10.1029/JA092iA03p02514>
- Blanc, M., & Richmond, A. D. (1980). The ionospheric disturbance dynamo. *Journal of Geophysical Research*, 85(A4), 1669–1686. <https://doi.org/10.1029/JA085iA04p01669>
- Bruinsma, S. L., & Forbes, J. M. (2007). Global observation of traveling atmospheric disturbances (TADs) in the thermosphere. *Geophysical Research Letters*, 34, L14103. <https://doi.org/10.1029/2007GL030243>
- Bulusu, J., Archana, R. K., Arora, K., Chandrasekhar, N. P., & Nagarajan, N. (2018). Effect of disturbance electric fields on equatorial electrojet over Indian longitudes. *Journal of Geophysical Research: Space Physics*, 123, 5894–5916. <https://doi.org/10.1029/2018JA025247>
- Burke, W. J., Gentile, L. C., Huang, C. Y., Valladares, C. E., & Su, S. Y. (2004). Longitudinal variability of equatorial plasma bubbles observed by DMSP and ROCSAT-1. *Journal of Geophysical Research*, 109, A12301. <https://doi.org/10.1029/2004JA010583>
- de La Beaujardière, O., & The C/NOFS Definition Team. (2004). C/NOFS: A mission to forecast scintillations. *Journal of Atmospheric and Solar-Terrestrial Physics*, 66, 1573–1591. <https://doi.org/10.1016/j.jastp.2004.07.030>

- Ebihara, Y., Tanaka, T., & Kikuchi, T. (2014). Counter equatorial electrojet and overshielding after substorm onset: Global MHD simulation study. *Journal of Geophysical Research: Space Physics*, *119*, 7281–7296. <https://doi.org/10.1002/2014JA020065>
- Foster, J. C., & Vo, H. B. (2002). Average characteristics and activity dependence of the subauroral polarization stream. *Journal of Geophysical Research*, *107*(A12), SIA16-1–SIA16-10. <https://doi.org/10.1029/2002JA009409>
- Fujiwara, H., & Miyoshi, Y. (2006). Characteristics of the large-scale traveling atmospheric disturbances during geomagnetically quiet and disturbed periods simulated by a whole atmosphere general circulation model. *Geophysical Research Letters*, *33*, L20108. <https://doi.org/10.1029/2006GL027103>
- Fuller-Rowell, T. J., Millward, G. H., Richmond, A. D., & Codrescu, M. V. (2002). Storm-time changes in the upper atmosphere at low latitudes. *Journal of Atmospheric and Solar-Terrestrial Physics*, *64*(12–14), 1383–1391.
- Gouin, P. (1962). Reversal of the magnetic daily variation at Addis Ababa. *Nature*, *193*(4821), 1145–1146. <https://doi.org/10.1038/1931145a0>
- Gouin, P., & Mayaud, P. N. (1967). A propos de l'existence possible d'un contre electrojet aux latitudes magnetiques equatoriales. *Annales Geophysicae*, *23*, 41–47.
- Heelis, R. A. (2004). Electrodynamics in the low and middle latitude ionosphere: A tutorial. *Journal of Atmospheric and Solar-Terrestrial Physics*, *66*, 825–838. <https://doi.org/10.1016/j.jastp.2004.01.034>
- Heelis, R. A., Lowell, J. K., & Spiro, R. W. (1982). A model of the high-latitude ionospheric convection pattern. *Journal of Geophysical Research*, *87*(A8), 6339–6345. <https://doi.org/10.1029/JA087iA08p06339>
- Huang, C.-M., Richmond, A. D., & Chen, M.-Q. (2005). Theoretical effects of geomagnetic activity on low-latitude ionospheric electric fields. *Journal of Geophysical Research*, *110*, A05312. <https://doi.org/10.1029/2004JA010994>
- Huang, C.-S. (2020). Westward plasma drifts in the nighttime equatorial ionosphere during severe magnetic storms: A new type of penetration electric fields caused by subauroral polarization stream. *Journal of Geophysical Research: Space Physics*, *125*, e2020JA028300. <https://doi.org/10.1029/2020JA028300>
- Jadhav, G., Rajaram, M., & Rajaram, R. (2002). A detailed study of equatorial electrojet phenomenon using Ørsted satellite observations. *Journal of Geophysical Research: Space Physics*, *107*(A8), S1A.
- Kikuchi, T., Hashimoto, K. K., Kitamura, T. I., Tachihara, H., & Fejer, B. (2003). Equatorial counter electrojets during substorms. *Journal of Geophysical Research: Space Physics*, *108*(A11).
- Kikuchi, T., Hashimoto, K. K., & Nozaki, K. (2008). Penetration of magnetospheric electric fields to the equator during a geomagnetic storm. *Journal of Geophysical Research*, *113*, A06214. <https://doi.org/10.1029/2007JA012628>
- Kikuchi, T., Lühr, H., Schlegel, K., Tachihara, H., Shinohara, M., & Kitamura, T. I. (2000). Penetration of auroral electric fields to the equator during a substorm. *Journal of Geophysical Research: Space Physics*, *105*(A10), 23251–23261.
- Liu, H., Doornbos, E., & Nakashima, J. (2016). Thermospheric wind observed by GOCE: Wind jets and seasonal variations. *Journal of Geophysical Research: Space Physics*, *121*, 6901–6913. <https://doi.org/10.1002/2016JA022938>
- Lühr, H., Rother, M., Häusler, K., Alken, P., & Maus, S. (2008). The influence of nonmigrating tides on the longitudinal variation of the equatorial electrojet. *Journal of Geophysical Research: Space Physics*, *113*(A8).
- Manoj, C., Maus, S., Lühr, H., & Alken, P. (2008). Penetration characteristics of the interplanetary electric field to the daytime equatorial ionosphere. *Journal of Geophysical Research*, *113*, A12310. <https://doi.org/10.1029/2008JA013381>
- Wan, X., Xiong, C., Rodriguez-Zuluaga, J., Kervalishvili, G. N., Stolle, C., & Wang, H. (2018). Climatology of the occurrence rate and amplitudes of local time distinguished equatorial plasma depletions observed by Swarm satellite. *Journal of Geophysical Research: Space physics*, *123*(4), 3014–3026.
- Wang, H., Lühr, H., Zheng, Z., & Zhang, K. (2019). Dependence of the equatorial electrojet on auroral activity and in situ solar insolation. *Journal of Geophysical Research: Space Physics*, *124*, 10659–10673. <https://doi.org/10.1029/2019JA027320>
- Wang, H., Ridley, A. J., Lühr, H., Liemohn, M. W., & Ma, S. Y. (2008). Statistical study of the subauroral polarization stream: Its dependence on the cross-polar cap potential and subauroral conductance. *Journal of Geophysical Research - A: Space Physics*, *113*(A12), A12311. <https://doi.org/10.1029/2008JA013529>
- Wang, W. B., Talaat, E. R., Burns, A. G., Emery, B., Hsieh, S. Y., Lei, J. H., & Xu, J. Y. (2012). Thermosphere and ionosphere response to subauroral polarization streams (SAPS): Model simulations. *Journal of Geophysical Research - A: Space Physics*, *117*(A7), A07301. <https://doi.org/10.1029/2012JA017656>
- Wu, Q., Sheng, C., Wang, W., Noto, J., Kerr, R., McCarthy, M., & Sarris, T. (2019). The midlatitude thermospheric dynamics from an interhemispheric perspective. *Journal of Geophysical Research: Space Physics*, *124*(10), 7971–7983.
- Yamazaki, Y., Harding, B. J., Stolle, C., & Matzka, J. (2021). Neutral wind profiles during periods of eastward and westward equatorial electrojet. *Geophysical Research Letters*, *48*, e2021GL093567. <https://doi.org/10.1029/2021GL093567>
- Yamazaki, Y., & Kosch, M. J. (2015). The equatorial electrojet during geomagnetic storms and substorms. *Journal of Geophysical Research: Space Physics*, *120*, 2276–2287. <https://doi.org/10.1002/2014JA020773>
- Yamazaki, Y., & Maute, A. (2017). Sq and EEJ—a review on the daily variation of the geomagnetic field caused by ionospheric dynamo currents. *Space Science Reviews*, *206*(1–4), 299–405.
- Yamazaki, Y., Stolle, C., Matzka, J., Siddiqui, T. A., Lühr, H., & Alken, P. (2017). Longitudinal variation of the lunar tide in the equatorial electrojet. *Journal of Geophysical Research: Space Physics*, *122*, 12445–12463. <https://doi.org/10.1002/2017JA024601>
- Yizengaw, E., & Moldwin, M. B. (2009). African meridian B-field education and research (AMBER) array. *Earth Moon Planet*, *104*(1), 237–246. <https://doi.org/10.1007/s11038-008-9287-2>
- Yizengaw, E., Moldwin, M. B., Mbrahtu, A., Dantie, B., Zesta, E., Valladares, C. E., & Doherty, P. (2011). Comparison of storm time equatorial ionospheric electrodynamic in the African and American sectors. *Journal of Atmospheric and Solar-Terrestrial Physics*, *73*(1), 156–163.
- Zhang, K., Liu, J., Wang, W., & Wang, H. (2019). The effects of IMF Bz periodic oscillations on thermospheric meridional winds. *Journal of Geophysical Research: Space Physics*, *124*, 5800–5815. <https://doi.org/10.1029/2019JA026527>
- Zhang, K. D., Wang, H., Wang, W. B., Liu, J., Zhang, S. R., & Sheng, C. (2021). Nighttime meridional neutral wind responses to SAPS simulated by the TIEGCM: A universal time effect. *Earth and Planetary Physics*, *5*(1), 52–62. <https://doi.org/10.26464/epp2021004>
- Zhang, K. D., Yamazaki, Y., Wang, H., & Xiong, C. (2021). Effects of subauroral polarization streams on the equatorial electrojet during the 1 June 2013 geomagnetic storm. *Journal of Geophysical Research: Space Physics*, *126*(10), e2021JA029681.
- Zheng, Z. C., Wang, H., Yu, L., He, Y. F., & Li, K. L. (2018). Temporal and spatial variations of the equatorial electrojet during storm time from CHAMP observations. *Journal of Atmospheric and Solar-Terrestrial Physics*, *179*, 307–315. <https://doi.org/10.1016/j.jastp.2018.07.012>